Journal of Colloid and Interface Science 653 (2024) 1478–1487

Contents lists available at ScienceDirect

Journal of Colloid And Interface Science

journal homepage: www.elsevier.com/locate/jcis

# Heating-induced adsorption promoting the efficient removal of toluene by the metal-organic framework UiO-66 (Zr) under visible light

Jiajun Yu [a,b], Xiao Wang [a], Yan Wang [a], Xiaofeng Xie [a], Haijiao Xie [c], Nat Vorayos [d], Jing Sun [a,*]

[a] *State Key Lab of High Performance Ceramics and Superfine Microstructure, Shanghai Institute of Ceramics, Chinese Academy of Sciences, 585 Heshuo Road, Shanghai 201899, China*

[b] *University of Chinese Academy of Sciences, 19 (A) Yuquan Road, Beijing 100049, China*

[c] *Hangzhou Yanqu Information Technology Co., No. 712 Wen'er West Road, Hangzhou, Zhejiang 310003, China*

[d] *Department of Mechanical Engineering, Faculty of Engineering, Chiang Mai University, Thailand*

## HIGHLIGHTS

- The unexpected efficient toluene removal by UiO-66 under visible light was studied.
- DFT showed that toluene was preferentially adsorbed on the metal center Zr.
- The heating-induced adsorption of UiO-66 to toluene was firstly revealed.
- Charge transfer between UiO-66 and adsorbed toluene extended the carrier lifetime.
- Synergic effect of heating-induced adsorption and photodegradation was proposed.

## GRAPHICAL ABSTRACT

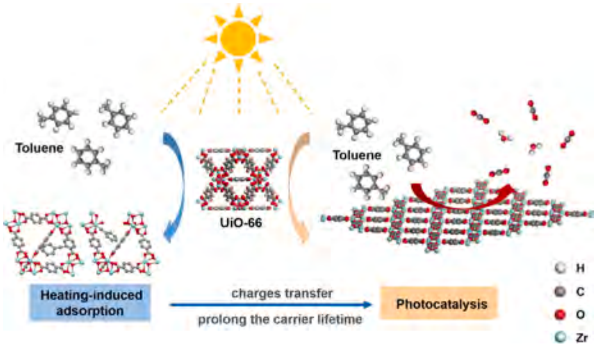

## ARTICLE INFO

*Keywords:*
UiO-66
Toluene
Heating-induced adsorption
DFT

## ABSTRACT

The removal of indoor/outdoor toluene by photocatalysis has drawn much attention due to its low energy consumption and easy availability. However, light inevitably generates heat, and pollutants desorb from catalysts as the temperature rises, which is not beneficial to degradation. Contrast to the frequently occurred phenomena, we firstly found that the adsorption capacity of UiO-66 (Zr) on toluene increased with increasing temperature as adsorption isotherms and in-situ Fourier transform infrared spectra (in-situ FTIR) showed. The optimum temperature was 30 °C. This stage in which adsorption capacity was positively correlated with temperature was called heating-induced adsorption, which achieved a toluene removal efficiency of 69.6 %. By density functional theory (DFT) calculations and changing the metal centers and organic ligands of UiO-66 (Zr) respectively, we disclosed that the heating-induced adsorption was mainly related to the π-π stacking interaction of MOF ligands and toluene. The analysis of samples before and after adsorption showed that the interaction between UiO-66 (Zr) and adsorbed toluene facilitated the charge transfer and prolonged the carrier lifetime, leading to the increase of hydroxyl radicals (•OH) in photocatalysis. Therefore, a synergistic effect between heating-induced adsorption and photocatalysis was proposed by analyzing the adsorption of toluene on UiO-66 (Zr) in detail.

---

* Corresponding author at: State Key Lab of High-Performance Ceramics and Superfine Microstructure, Shanghai Institute of Ceramics, Chinese Academy of Sciences, 585 Heshuo Road, Shanghai 201899, China.

*E-mail address:* jingsun@mail.sic.ac.cn (J. Sun).

https://doi.org/10.1016/j.jcis.2023.09.164
Received 16 July 2023; Received in revised form 13 September 2023; Accepted 27 September 2023

This work provided new viewpoint to understand the role of concomitant heat contributed to the adsorption and degradation of toluene during photocatalysis.

## 1. Introduction

People nowadays spend more than 80 % of their time in indoor spaces [1]. The continuous release of volatile organic compounds (VOCs) by interior decorations, building materials (such as adhesives, and coatings), and furniture brings great harm to human health [2,3]. Some aromatic VOCs such as benzene and toluene have even been classified as carcinogens [4]. Therefore, the treatment of aromatic hydrocarbons is of great significance for indoor air purification.

The removal methods of VOCs are mainly divided into three categories. One is the combustion method for treating waste gas [5]. The second is the use of adsorbents to absorb VOCs [6]. The third is catalytic oxidation [7]. The combustion method is often used to treat high concentration of industrial waste gas, with high energy consumption. The latter two methods are mainly used to remove low concentration of VOCs in daily life. Among them, photocatalytic oxidation (PCO) has been regarded as a promising means to eliminate indoor VOCs [8,9], because of its advantages such as mild reaction conditions (ambient temperature and pressure), low energy consumption, and no equipment dependency. Metal-organic frameworks (MOFs) are a kind of porous crystalline nanomaterials which are consisted of inorganic units (metal ions or metal clusters) connected by polytopic organic ligands [10]. With a large specific surface area, high porosity along with easily regulated pore structure and chemical composition [11], MOFs are widely used in molecular adsorption and separation [12–14], fluorescence sensing [15,16], and catalysis [17–19], etc. Guo et al. [20] reviewed the mechanism and research progress of peroxymonosulfate (PMS) activation on Zeolitic imidazolate framework (ZIF)-based materials for the removal of organic pollutants. Xiao et al. [21] systematically discussed the preparation of MOFs-derived metal/carbon composites and their applications in catalysis and energy. As one kind of zirconium-based MOF structure, UiO-66 (Zr) not only has the same superior properties (e.g. a large specific surface area, and adjustable pore structures) as other MOFs, but also exhibits better water/air stability, strong acid resistance [22], and photocatalytic activity, which make it a promising candidate for VOCs removal [23].

At present, in order to make the photocatalyst more widely used in daily life, researchers are working on adjusting the light absorption range of the catalysts and improving the catalytic efficiency under visible light [18,24,25]. It is well known that light inevitably releases heat, which increases the temperature of the catalysts. By reviewing some papers on the adsorption of VOCs by MOFs [26,27], the adsorption capacity of most adsorbents for VOCs decreased as the temperature increased. The adsorption process is a critical step in gas-phase catalysis, significantly affecting the catalytic efficiency. Therefore, the heat generated by light increases the temperature of the catalysts, which will inevitably affect the adsorption and degradation of VOCs. However, whether this is a positive or negative effect remains to be explored, and there are few research reports.

In this work, toluene was selected as the representative of VOCs. The temperature change of the reaction chamber was recorded under visible light irradiation. Subsequently, the light source was removed and the reaction chamber was heated to simulate the temperature change during illumination. Toluene concentration was recorded to explore the adsorption of toluene by UiO-66 (Zr) in the temperature range of illumination. In-situ Fourier transform infrared spectra (in-situ FTIR), density functional theory (DFT) calculations, and toluene adsorption isotherms of UiO-66 (Zr) at different temperatures were tested to further explore the adsorption behavior and the effect of light-induced temperature change on the toluene adsorption. It was found that the adsorption capacity of UiO-66 (Zr) on toluene increased first and then decreased with the increase of temperature. In response to the phenomenon of increased adsorption capacity (called heating-induced adsorption), the metal and ligand species of UiO-66 (Zr) were respectively changed, and UiO-66 (Hf) and MOF-801 were selected as control groups to explore the interaction between MOFs and toluene. Heating-induced adsorption was found to be related to the π-π stacking interaction of MOFs and toluene. In addition, samples before and after adsorption were selected for X-ray photoelectron spectroscopy (XPS), transient fluorescence spectroscopy, electron spin resonance (ESR), and other tests, in order to further explore the influence of adsorption on the catalysts and catalytic process. Charge transfer between adsorbed toluene and UiO-66(Zr) was found, which prolonged the carrier lifetime and increased the number of hydroxyl radicals (•OH). This work first found that heating-induced adsorption was a key factor in promoting the removal of toluene by UiO-66 (Zr). The heating-induced adsorption of UiO-66 (Zr) was mainly caused by π-π stacking interaction between the benzene ring and toluene. The synergistic effect between heating-induced adsorption and photocatalysis was proposed for the first time. In addition, the effect of adsorption on photogenerated carrier separation and free radical generation was investigated.

## 2. Experimental section

### 2.1. Materials

Zirconium tetrachloride ($ZrCl_4$, ≥99.9 %), hafnium tetrachloride ($HfCl_4$, 99.5 %), ethyl alcohol (EtOH, ≥99.7 %), and 5,5-dimethyl-1-pyrroline *N*-oxide (DMPO, 99.0 %) were purchased from Shanghai Aladdin Co., Ltd. N, *N*-dimethylformamide (DMF, $C_3H_7NO$, 99.5 %), terephthalic acid ($H_2BDC$, $C_8H_6O_4$, 99.0 %), L-aspartic acid ($C_4H_7NO_4$, 98 %), methanol ($CH_3OH$, 99.9 %) and fumaric acid ($C_4H_4O_4$, 99.0 %) were purchased from Adamas Corporation. Titanium (IV) butoxide ($C_{16}H_{36}O_4Ti$, ≥98.5 %) was purchased from General-Reagent Corporation.

### 2.2. Samples preparation

#### 2.2.1. Synthesis of UiO-66 (Zr)

Based on the previous report [22], UiO-66 (Zr) was synthesized by a solvothermal method. $ZrCl_4$ (1.0 mmol) and $H_2BDC$ (1.0 mmol) were dissolved in DMF (50 mL), and then the mixed solution was stirred for 45 min. The solution was placed in 100 mL autoclave and kept at 120 °C for 24 h. The precipitate was washed and then dried at 80 °C for 8 h in a vacuum.

#### 2.2.2. Synthesis of UiO-66 (Hf)

According to the previous report [28], $HfCl_4$ (1.0 mmol) and $H_2BDC$ (1.0 mmol) were dissolved in DMF (50 mL), and the rest steps were the same as the synthesis of UiO-66 (Zr).

#### 2.2.3. Synthesis of MOF-801

From the previous report [29], $ZrCl_4$ (1.0 mmol) and fumaric acid (1.0 mmol) were dissolved in DMF (50 mL), and the next steps were the same as the synthesis of UiO-66 (Zr).

#### 2.2.4. Synthesis of MIP-202

From the previous report [30], L-aspartic acid (2.8 g) and $ZrCl_4$ (2.33 g) were transferred to a 25 mL round bottom flask. 10 mL of water was added. The reaction was kept at reflux for 1 h (120 °C). After cooling to room temperature, the sample was washed with ethanol and dried at room temperature for 24 h.

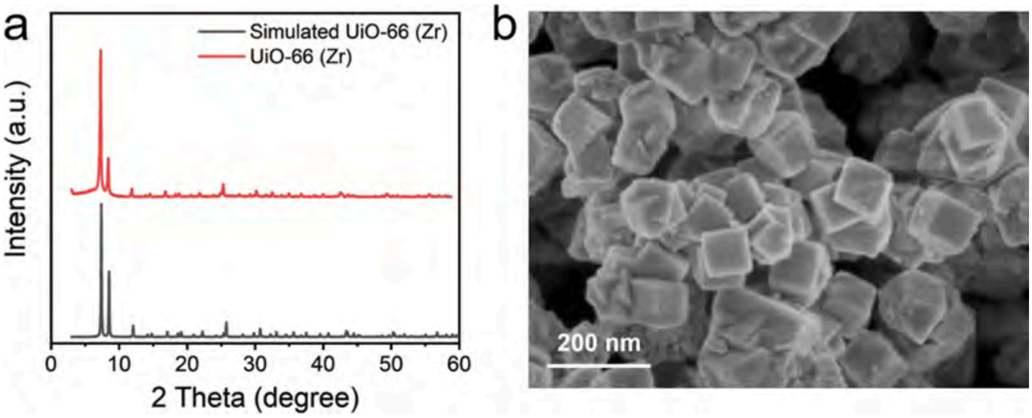

**Fig. 1.** The (a) XRD patterns and (b) SEM image of UiO-66 (Zr).

#### 2.2.5. *Synthesis of MIL-125 (Ti)*

From the previous report [31], 7.5 g $H_2BDC$ was dissolved in 100 mL DMF and 25 mL methanol and stirred for 1 h. Then 7.5 mL of Titanium (IV) butoxide was added. The reaction was carried out at 150 °C for 16 h. At room temperature, the solid was washed with DMF and ethanol, respectively, and dried at 80 °C for 10 h.

### 2.3. *Characterization*

The morphology of the samples was observed by scanning electron microscope (SEM, FEI Magellan 400). X-ray diffractometer (XRD, Bruker, Germany) with Cu $K_\alpha$ irradiation, was used to characterize the structure of the samples. A specific surface pore size analyzer (Quanta Instruments, Inc.) was used to measure the specific surface area of the samples. The toluene adsorption curves of the samples were measured using a specific surface aperture analyzer (Bayer MAX2). The surface valence states of the samples were researched by X-ray photoelectron spectroscopy (XPS, ESCAlab250). The adsorption sites of the samples were researched by a chemical adsorption analyzer (Builder Electronic Technology). The recombination degree of photogenerated carriers in samples was researched by a luminescence spectrometer (Perkin Elmer). A transient fluorescence spectrometer (Edinburgh, FLS980) was used to analyze the fluorescence lifetime. A digital display electric heating plate (C-MAG HP10, Ika) was used to control the temperature change in the reaction chamber. A gas chromatograph (GC-7920, Beijing Zhongjiao Jinyuang Co., Ltd.) was used to monitor the concentrations of toluene and $CO_2$.

### 2.4. *Photocatalytic performance measurements*

The S1 scheme showed the device for photocatalytic degradation of toluene in experiments, which automatically and continuously fed the pollutants [32]. The light source was 250 W ($\lambda > 400$ nm). A glass slide (75 mm × 150 mm) coated with 30 mg catalyst and a thermometer were placed in the reaction chamber. Firstly, toluene (20 ppm, 20 sccm) and air (20 sccm) flowed over the catalyst surface in a dark environment until the toluene concentration was constant. A gas chromatograph was used to detect the toluene concentration every 10 min. Then the light was turned on, and the temperature was recorded every 10 min.

The removal ratio (η) of toluene was enumerated according to the equation:

$$\eta = (1 - \frac{C}{C_0}) \times 100\%$$

The saturated adsorption capacity (A, μmol/g) was calculated as follows:

$$A = \left\{ \left[ \int_0^t \left( \frac{C_0 - C}{C_0} \right) dt \right]_{sample} - \left[ \int_0^t \left( \frac{C_0 - C}{C_0} \right) dt \right]_{blank} \right\} \times C_0 \times v \times (M \times m)^{-1}$$

where $C_0$ and C are the initial and actual concentrations of pollutants, respectively. The flow rate of toluene is “v”. The mass of the catalyst and the molar mass of the contaminated gas are denoted by m and M, respectively.

### 2.5. *Control experiment*

The light source of the above-mentioned photocatalytic process was removed. The reaction chamber was connected to the circulating water and a digital display electric heating plate was applied to regulate the temperature of the reaction chamber. After the catalyst reached the adsorption–desorption equilibrium in the dark, the heating plate was turned on to heat the reaction chamber, to simulate the temperature change during the process of illumination. The temperature was recorded every 10 min and the concentration of toluene was recorded every 10 min.

### 2.6. *ESR tests*

The contents of •OH and were determined by electron spin resonance (ESR, Bruker EMXplus-6/1, Germany). The samples were tested separately by ESR after 10 min of light irradiation ($\lambda > 400$ nm).

### 2.7. *Computational methods*

Density functional theory (DFT) calculations were performed using the Vienna ab initio Simulation Package (VASP) [33]. The generalized gradient approximations (GGA) of Perdew-Burke-Ernzerhof (PBE) [34] and the projector-augmented-wave (PAW) [35] potentials were chosen for the exchange-correlated generalization function. The total energy convergence criterion was $10^{-4}$ eV. The atomic positions were relaxed by using the conjugate gradient algorithm until the forces on the atoms were less than 0.05 eV/Å. The plane-wave kinetic energy cutoff was set to 500 eV. The k-points were set to 1 × 1 × 1. The empirical correction in Grimme’s Scheme was used to describe the van der Waals interactions. The three-dimensional structures were visualized by the visualization for electronic and structural analysis (VESTA) code [36].

## 3. Results and discussion

### 3.1. *Morphological and structural characterization*

Fig. 1a showed the XRD pattern of the synthesized UiO-66 (Zr)

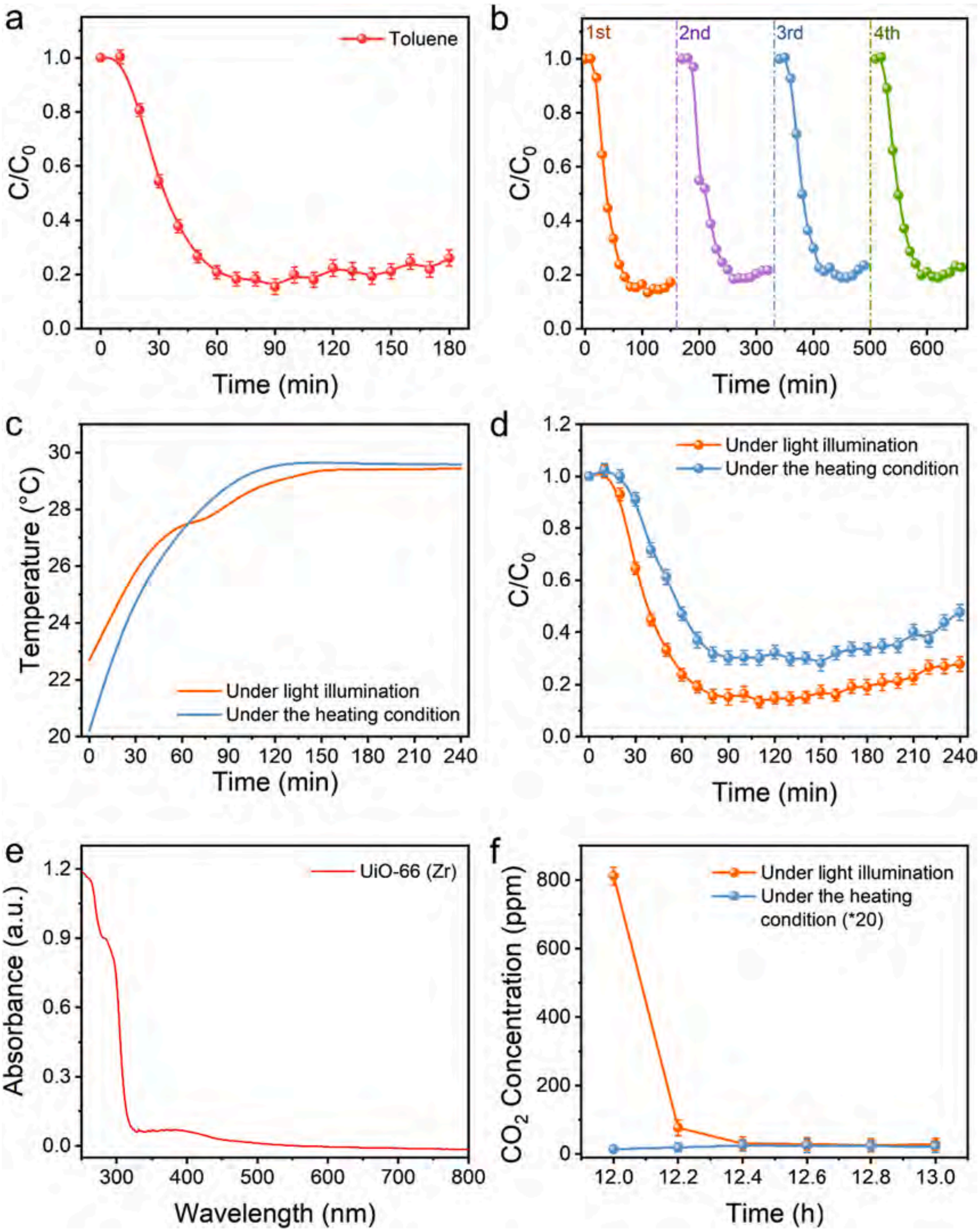

**Fig. 2.** Gaseous toluene removal curves by UiO-66 (Zr) under visible light irradiation for (a) 180 min and (b) four cycles. (c) The real-time temperature change curves under different environments. (d) Toluene removal curves of UiO-66 (Zr) in the experiment (c). (e) Ultraviolet–visible absorption spectrum. (f) The concentration of $CO_2$ produced in the process of the toluene removal using UiO-66 (Zr) under different conditions. The error bars in the figure were calculated from three repeated experiments.

sample. The peak positions of this material were in a good agreement with the simulated ones [37]. The sharp diffraction peaks indicated the good crystallinity of the UiO-66 sample, which was also seen from the SEM image (Fig. 1b). Fig. S1 showed a type I $N_2$ adsorption–desorption isotherms [38], confirming the persistent micropores inside UiO-66 (Zr). The specific surface area of the prepared UiO-66 (Zr) was 854 $m^2/g$ (Table S1), which was consistent with previous papers [39,40]. These results showed that UiO-66 (Zr) was successfully synthesized.

### 3.2. Toluene removal by UiO-66 (Zr) under visible light

Fig. 2a showed the toluene removal curve of UiO-66 (Zr) under visible light irradiation, with a maximum toluene removal efficiency of 91.2 % in 90 min. Almost no performance decay was observed in four-cycle tests (Fig. 2b), confirming the high stability of UiO-66 (Zr) in toluene removal. UiO-66 (Zr) was a semiconductor with a wide bandgap, and its response to visible light was very weak. So where did such a remarkable toluene removal efficiency come from? It was worth exploring. As is well known, light inevitably generates heat, which may

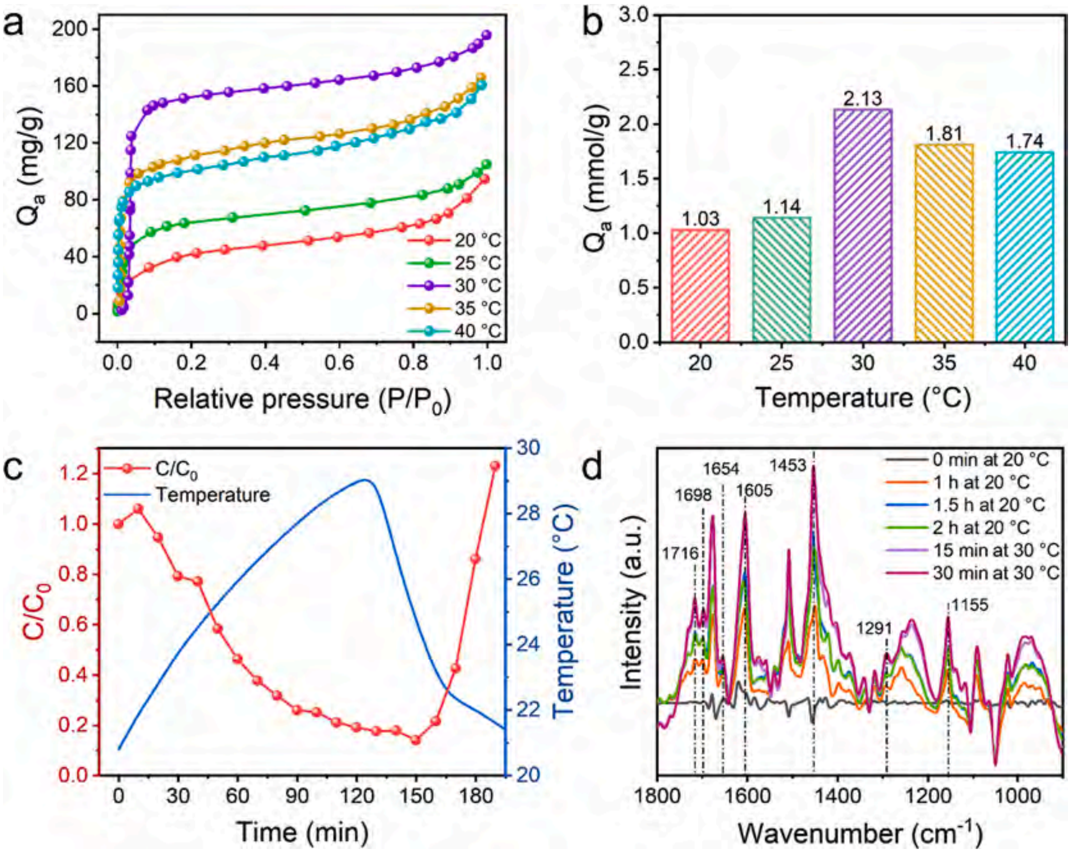

**Fig. 3.** (a) Adsorption isotherms and (b) corresponding adsorption capacity of UiO-66 (Zr) for toluene under different temperatures. (c) The curve of the toluene removal using UiO-66 (Zr) at continuous temperature variation. (d) In-situ FTIR differential spectra of toluene adsorption by UiO-66 (Zr) at 20 °C and 30 °C. (The original signal of UiO-66 was subtracted.)

increase the temperature of the catalysts. In order to elucidate the effect of heat on adsorption and degradation, a separate heater was introduced into the reaction chamber to mimic the temperature change under light illumination. The toluene concentration change was compared. Fig. 2c showed that the temperature profile changes consistently after 90 min. Keeping the temperature basically the same, we found that there were different toluene removal efficiencies, 91.2 % and 69.6 %, respectively (Fig. 2d). It could be seen that the increase in temperature from 20 °C to 30 °C resulted in a toluene removal efficiency of 69.6 %. It was speculated that temperature rise may increase the adsorption capacity of the catalyst to toluene, which will be discussed in detail in Section 3.3. There was 91.2 % toluene removal under light illumination, and 21 % removal contribution was speculated to result from photocatalysis. Then, the ultraviolet –visible absorption spectrum of UiO-66 (Zr) was tested (Fig. 2e) and it had weak visible light absorption. We further detected the concentration of $CO_2$ under light illumination. The whole reaction chamber and the gas path were sealed for 12 h. The $CO_2$ adsorbed by the catalyst was blown out with $N_2$. Fig. 2f showed the concentration of $CO_2$ detected by purging the reaction chamber with $N_2$ after 5 h of illumination. The high $CO_2$ concentration (811.83 ppm) proved that toluene was decomposed by UiO-66 (Zr) through photocatalysis.

Through previous papers, it was found that Xu et al. [41] measured the photocurrent response of UiO-66 (Zr) under visible light. Xiao et al. [42], Yi et al. [43], and Dong et al. [44] respectively measured the efficiency of UiO-66 (Zr) catalyzing benzyl alcohol, reducing Cr (VI) and removing tetracycline under visible light. Wu et al. [40] found that UiO-66 (Zr) always contained defects. With the increase of defect concentration, UiO-66 showed color changes, suggesting that the defect might change the electron band structure of UiO-66 (Zr). We speculated that defects in UiO-66 (Zr) produced defect energy levels, and affected electron transition and light absorption, so there was a weak visible light response, but this work does not discuss it in depth. In this work, the effect of temperature on the adsorption of toluene by UiO-66 (Zr) was studied.

To clarify the influence of temperature on the removal of toluene and explore whether thermal degradation occurred, the concentration of $CO_2$ was detected after heating the reaction system for 5 h. For visualization, the $CO_2$ concentration was enlarged by a factor of 20 and compared with illumination (Fig. 2f). In Fig. 2f, almost no $CO_2$ (1.3 ppm) was produced under the heating condition, which indicated that no degradation of toluene occurred under pure heating. This confirmed that the decrease in the toluene concentration during heating was mainly related to the adsorption.

### *3.3. The effect of temperature on toluene adsorption by UiO-66 (Zr)*

To further explore the influence of temperature on the toluene adsorption, the toluene adsorption isotherms were detected under different temperatures. According to the temperature range (20–40 °C) shown in Fig. 2c, the adsorption isotherms of UiO-66 (Zr) were tested at different temperatures at intervals of 5 °C. As the temperature increased, the amount of toluene adsorbed in UiO-66 (Zr) firstly increased from 20 °C to 30 °C and then decreased a little from 30 °C to 40 °C. Fig. 3a–b showed that 30 °C was the optimal adsorption temperature, and the corresponding adsorption capacity was 2.13 mmol/g. This temperature-dependent adsorption capacity (known as heating-induced adsorption) might be the main reason for the heating-induced toluene removal by UiO-66 (Zr). To verify this conjecture, after UiO-66 (Zr) reached the adsorption–desorption equilibrium at 20 °C, continuous temperature-

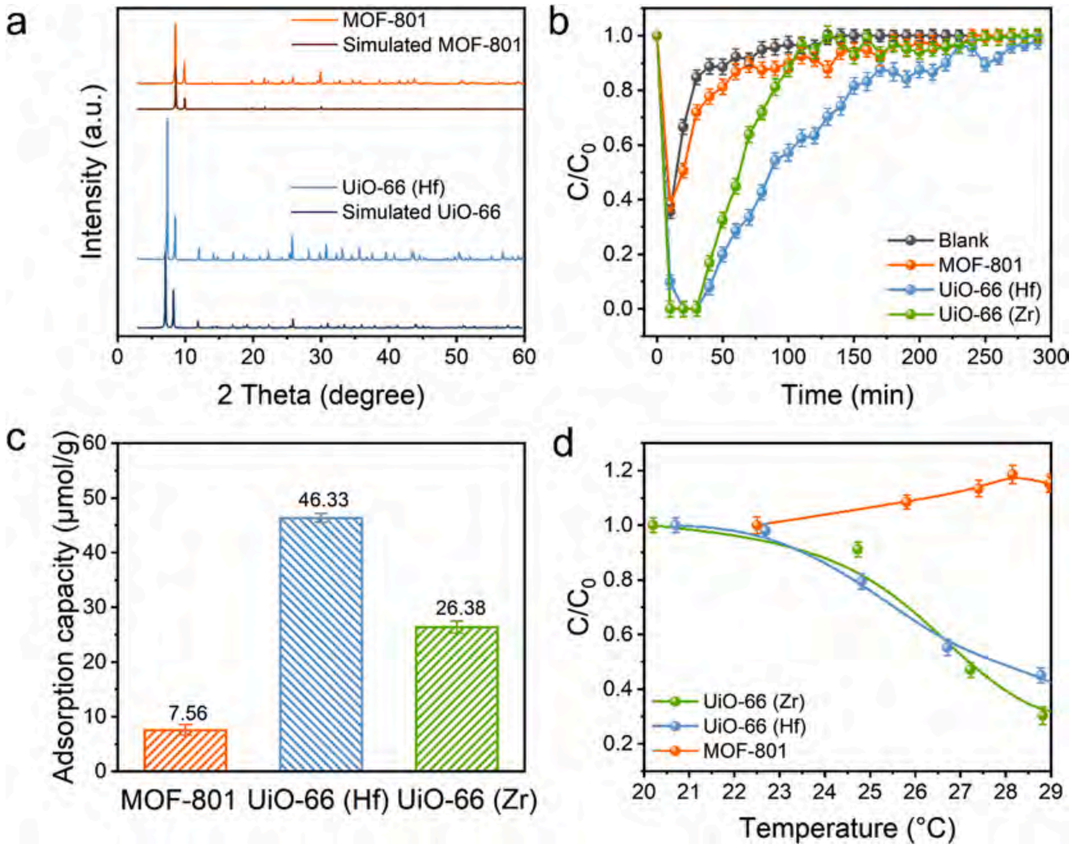

**Fig. 4.** (a) The XRD patterns, (b) Adsorption curves, and (c) The saturated adsorption capacity of flowing gaseous toluene for different MOF samples in dark conditions. (d) Gaseous toluene concentration curves using different MOF samples under heating. The error bars in the figure were calculated from three repeated experiments.

varying experiments from 20 °C to 30 °C were performed while monitoring the toluene concentration. Fig. 3c showed that the toluene concentration decreased with temperature during the first 130 min, indicating the enhanced adsorption amount of toluene with increasing temperature from 20 °C to 30 °C. Within 130–190 min, as the temperature decreased from 30 °C to 21 °C, the adsorption capacity for toluene of UiO-66 (Zr) decreased, and toluene was desorbed from the sample, leading to $C/C_0$ more than 1. This indicated that the toluene was stored in UiO-66 (Zr) during the heating-induced adsorption and was released by cooling. In addition, the existence of heating-induced adsorption was further confirmed by in-situ FTIR differential spectra (Fig. 3d). UiO-66 (Zr) initially adsorbed toluene at 20 °C. As shown in Fig. 3d, the peak at 1453 $cm^{-1}$ was caused by $\nu$ (OH) vibration in the aromatic ring [45]. The peak at 1716 $cm^{-1}$ was attributed to the $\nu$ (C═O) vibration of the aromatic group [45,46]. 1650, 1597 and 1543 $cm^{-1}$ were attributed to the vibration of $\nu$ (C═C) of the benzene ring skeleton [47]. The peak at 1291 $cm^{-1}$ was designated as $\nu$ (C—O—C) vibration [48]. The peak at 1161 $cm^{-1}$ was attributed to the $\nu$ (C—OH) vibration [49]. 1450–1650 $cm^{-1}$ was attributed to the skeleton vibration of C═C in the benzene ring [47]. The signal intensity reflected the toluene adsorption capacity of UiO-66 (Zr). The signal intensity of 1.5 h and 2 h almost did not change, indicating the adsorption saturation. Then UiO-66 (Zr) was heated to 30 °C in-situ. It was found that the signal intensity increased obviously after 15 min, indicating more adsorption occurred and reached saturation again at 30 min. The above results proved the existence of heating-induced adsorption.

As reported previously by Chen et al. [50], both metal centers and ligands in MOFs could work as active sites for the adsorption of guest molecules. In order to explore the original factors causing heating-induced adsorption, control experiments were carried out. By altering the metal center from Zr to Hf or the ligand from benzene-ring containing $H_2BDC$ to fumaric acid, UiO-66 (Hf) and MOF-801 were synthesized for comparison. The XRD patterns (Fig. 4a) confirmed the successive synthesis of UiO-66 (Hf) and MOF-801.

As shown in Fig. 4b, the catalysts reached adsorption–desorption equilibrium in the dark, and the toluene adsorption capacity of different catalysts was calculated (Fig. 4c). Both UiO-66 materials with benzene rings-containing ligands showed high toluene adsorption capacity. Despite the relatively smaller surface area of as-prepared UiO-66 (Hf) (686 $m^2/g$), it exhibited stronger adsorption capacity towards toluene than UiO-66 (Zr) (854 $m^2/g$). According to the previous paper [28], UiO-66 (Hf) and UiO-66 (Zr) had similar structures and physical properties. The improved toluene adsorption performance might be related to the relatively stronger Lewis acidity of UiO-66 (Hf), which promoted the adsorption of toluene (Lewis base) [51]. Even though MOF-801 also exhibited a high specific surface area (563 $m^2/g$), its toluene adsorption capacity was only 7.56 μmol/g. As proven by Chen et al. [50], π-π stacking interactions between toluene and the ligands containing benzene rings played an important part in the toluene adsorption. The lack of π-π interactions between toluene and MOF-801 with fumarate ligands might be a key reason for the limited adsorption capacity. Next, the toluene concentrations using UiO-66 (Hf) and MOF-801 samples under heating were tested (Fig. 4d). After reaching the toluene adsorption–desorption equilibrium in dark conditions at the room-temperature, the samples were all heated to 29 °C and the concentrations of toluene in the chamber were tested. UiO-66 (Zr) and UiO-66 (Hf) exhibited obvious heating-induced adsorption phenomena. However, toluene was continuously desorbed from MOF-801 during the heating. In addition, MIP-202 (Zr as the metal centers, L-aspartic acid as the ligands) and MIL-125 (Ti) (Ti as the metal centers, $H_2BDC$ as the ligands) were synthesized, and the XRD patterns were shown in Fig. S2a. The two samples which reached the adsorption–desorption equilibrium were

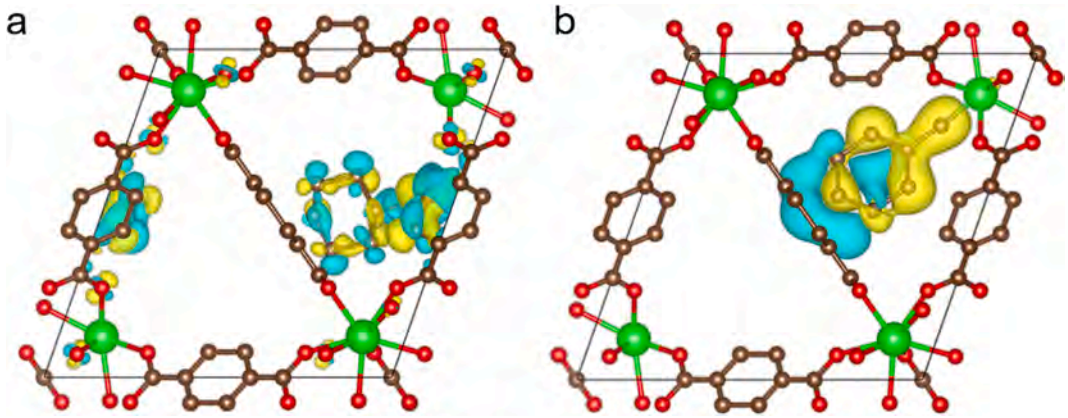

**Fig. 5.** Differential charge density of toluene adsorbed on (a) BDC and (b) metal center Zr. (Yellow represents the electron-rich zone and blue represents electron depletion.). (For interpretation of the references to color in this figure legend, the reader is referred to the web version of this article.)

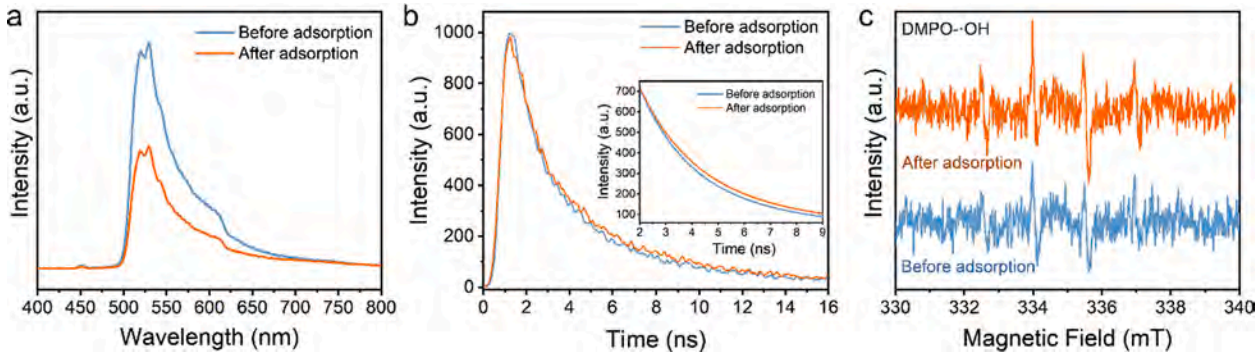

**Fig. 6.** (a) The photoluminescence spectra (PL) excited by 400 nm light, (b) The transient fluorescence spectra excited by 475 nm light, and (c) ESR spectra of DMPO-•OH before and after adsorption of toluene by UiO-66 (Zr).

heated. As shown in Fig. S2b, toluene was continuously desorbed from MIP-202 during the heating, while MIL-125 (Ti) exhibited heating-induced adsorption, confirming the importance of ligands during the heating-induced adsorption of toluene. Therefore, it was believed that the heating-induced adsorption phenomenon was mainly related to the organic ligands of MOFs rather than the metal centers. The π-π stacking interaction between the UiO-66 ligand containing benzene ring and toluene might play an important role. To verify this conjecture, DFT calculations were performed to compare the adsorption of toluene to metal centers and organic ligands.

Both the metal nodes and ligands may work as active sites for the adsorption of toluene. Therefore, toluene adsorption on $H_2BDC$ ligand (model 1) and Zr centers (model 2) of UiO-66 (Zr) were constructed, respectively. The adsorption energies and differential charge densities of the two adsorption models were compared. The adsorption energies of models 1 and 2 were −0.861 eV, and −2.206 eV, respectively. Model 1 required more energy than Model 2. Therefore, in the dark adsorption stage of the experiment, toluene was preferentially adsorbed on the metal center Zr until saturation. On the one hand, the heat generated by light could provide energy for the adsorption of toluene on UiO-66 (Zr) ligands. On the other hand, as heating could promote the mass-transfer of toluene in the pores of MOFs, the interaction between toluene and ligand adsorption sites in UiO-66 (Zr) and UiO-66 (Hf) might be promoted, and then heating-induced adsorption occurred. Furthermore, in Fig. 5a, the electron distribution indicated electron transfer between $H_2BDC$ and toluene. Fig. 5b clearly showed that toluene was in an electron-rich state. This indicated the existence of charge transfer between UiO-66 (Zr) and adsorbed toluene. The charge transfer in the adsorption stage might have an impact on photocatalysis, which was discussed in the next section.

**Table 1**
Decay lifetimes of transient fluorescence spectra and their relative percentages of photoexcited charge carriers in UiO-66 (Zr).

| Samples | $\tau_1$ (ns)[a] | $A_1$%[b] | $\tau_2$ (ns) | $A_2$% |
|---|---|---|---|---|
| UiO-66 (Zr)-before adsorption | 1.9 | 46.7 | 7.2 | 53.3 |
| UiO-66 (Zr)-after adsorption | 2.1 | 44.8 | 7.9 | 55.3 |

[a] τ referred to decay lifetime.
[b] A represented relative percentages.

### 3.4. The interrelationship between adsorption and catalysis

In order to investigate the effect of adsorption on photocatalysis, the samples before and after adsorption were characterized. According to XPS (Fig. S3), there was charge transfer between toluene and UiO-66 (Zr). The Zr peaks belonging to UiO-66 (Zr) structure shifted to a higher binding energy after adsorbing toluene, indicating the charge transfer from Zr centers to absorbed toluene [52]. Toluene adsorbed on Zr was in the electron-rich zone as also confirmed by the DFT (Fig. 5b). The photoluminescence spectra (PL) spectra (Fig. 6a) and transient fluorescence spectra (Fig. 6b) were further measured and the fluorescence lifetimes were analyzed (Table 1). Fig. 6a showed that the PL intensity of UiO-66 (Zr) decreased after adsorbing toluene, indicating that charge transfer between UiO-66 (Zr) and toluene reduced the recombination rate of photogenerated carriers. Fig. 6b showed that the fluorescence lifetime of UiO-66 (Zr) with adsorbed toluene was prolonged, which was also reflected in Table 1.

Table 1 showed that the carrier lifetime of UiO-66 (Zr) was prolonged after adsorbing toluene, and the proportion of long-lived carriers increased. Both the metal cluster-toluene and π-π stacking interactions

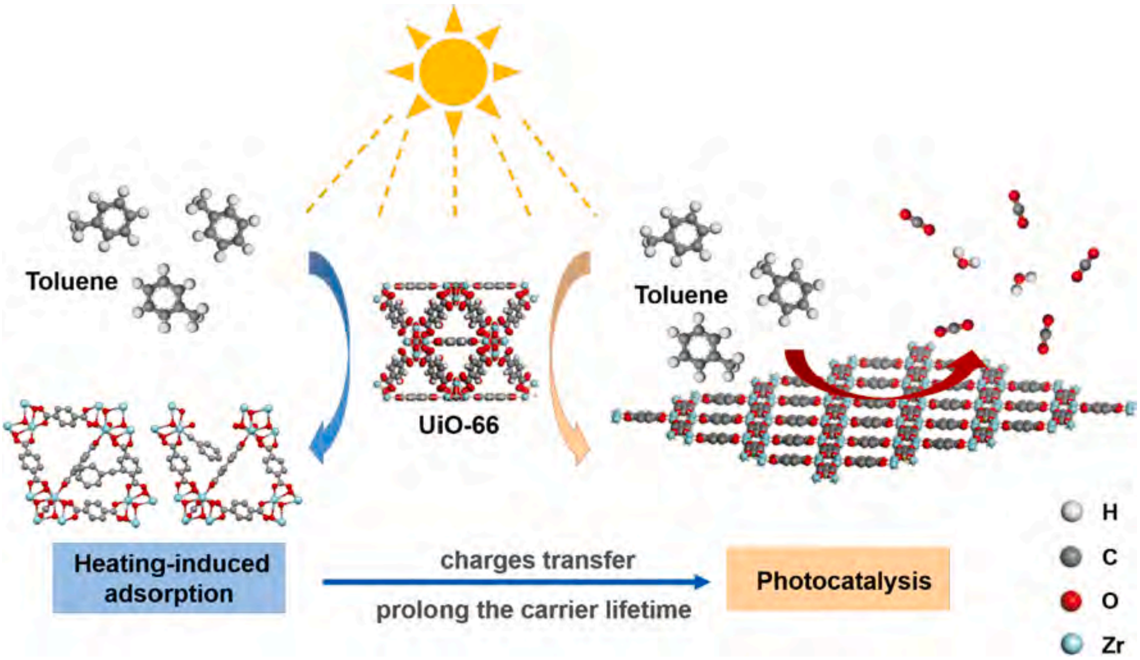

**Fig. 7.** Schematic diagram of the reaction.

promoted the charge transfer between UiO-66 (Zr) and toluene and thus prolonged the carrier lifetime. The prolongation of carrier lifetime was conducive to its migration to the surface of UiO-66 (Zr) to participate in the generation of more free radicals [53]. Previous results showed that hydroxyl radical (•OH) was the main active species in the toluene degradation [54]. For UiO-66 (Zr) adsorbed with toluene, the signals of •OH increased significantly (Fig. 6c), which was conducive to the mineralization of toluene [55]. The above results indicated that the interaction between adsorbed toluene and the catalyst provided a bridge for the separation of carriers, thus promoting radical generation and photodegradation.

Combing the theoretical and experimental results, the synergic effect between heating-induced adsorption and photocatalytic degradation could be proposed (Fig. 7). Toluene could be adsorbed by interacting with metals and ligands in UiO-66 (Zr). On the one hand, photocatalysis generated free radicals to promote degradation, and more adsorption sites could be exposed after toluene was degraded, which was favorable for adsorption. On the other hand, the adsorption of toluene by UiO-66 (Zr) increased with the increase of temperature caused by light irradiation. Meanwhile, the adsorption between UiO-66 (Zr) and toluene could prolong the lifetime of photogenerated charges and promote the generation of free radicals, which was favorable for photocatalysis.

## 4. Conclusion

In summary, a removal efficiency of 91.2 % was achieved during the photocatalytic degradation of toluene by UiO-66 (Zr) under visible light. Despite a variety of papers have reported similar results [41–44], the reasons for the visible light activity have not been explored. Herein, a novel mechanism of the visible-light induced photocatalytic removal of VOCs by MOFs was proposed and heating-induced adsorption was firstly found as a key factor in promoting the removal of toluene. Under the irradiation of visible light, the temperature of UiO-66 (Zr) gradually increased from room temperature to about 30 °C, which was proven to be the optimum temperature for toluene adsorption. Control experiments and theoretical calculation results revealed that the heating-induced adsorption was mainly attributed to the $\pi$-$\pi$ stacking interaction between UiO-66 (Zr) ligands containing benzene ring and toluene. A synergistic effect between heating-induced adsorption and photocatalysis was also proposed for the first time. On one hand, the heating-induced adsorption of toluene facilitated the charge transfer and prolonged the carrier lifetime, leading to an increase in the amount of oxidative •OH radicals for the degradation of toluene. On the other hand, the photocatalytic removal of toluene further provided new active sites for the adsorption of toluene. What has been found in this work would shed light on the design and optimization of new materials and processes for air decontamination. In the future work, the heat adsorption mechanism of other VOCs like acetaldehydes, alkane, alkene, et al. will be investigated. Besides, optimization would be carried out on UiO-66 (Zr) to further improve its heating-induced adsorption capacity and achieve its practical application.

## CRediT authorship contribution statement

**Jiajun Yu:** Investigation, Methodology, Validation, Writing – original draft, Writing – review & editing. **Xiao Wang:** Investigation, Methodology, Writing – review & editing. **Yan Wang:** Project administration, Funding acquisition. **Xiaofeng Xie:** Supervision, Project administration. **Haijiao Xie:** Methodology. **Nat Vorayos:** Supervision, Project administration. **Jing Sun:** Writing – review & editing, Supervision, Project administration, Funding acquisition.

## Declaration of Competing Interest

The authors declare that they have no known competing financial interests or personal relationships that could have appeared to influence the work reported in this paper.

## Data availability

Data will be made available on request.

## Acknowledgment

This work was financially supported by the National Key Research and Development Program of China (2021YFE0110400); the National Natural Science Foundation of China (52072387); the Natural Science Foundation of Shanghai (22ZR1471800); the Key Collaborative

Research Program of the Alliance of International Science Organization (ANSO-CR-KP-2020-13) and the Shanghai Commission of Science and Technology Program (19DZ1205102).

## Appendix A. Supplementary material

Supplementary data to this article can be found online at https://doi.org/10.1016/j.jcis.2023.09.164.

## References

[1] A. Okada, K. Sekiguchi, K. Sankoda, Mechanisms for removal of gaseous toluene in headspace using sonophysical and sonochemical effects at the gas-liquid interface, J. Hazard. Mater. 423 (2022).

[2] J. Zhang, K. Vikrant, K.-H. Kim, F. Dong, M.W. Chung, S. Weon, Unveiling the collective effects of moisture and oxygen on the photocatalytic degradation of m-Xylene using a titanium dioxide supported platinum catalyst, Chem. Eng. J. 439 (2022).

[3] R. Chen, J. Li, J. Sheng, W. Cui, X.a. Dong, P. Chen, H. Wang, Y. Sun, F. Dong, Unveiling the unconventional roles of methyl number on the ring-opening barrier in photocatalytic decomposition of benzene, toluene and o-xylene, Appl. Catal. B-Environ. 278 (2020).

[4] J. Chen, Y. Yang, S. Zhao, F. Bi, L. Song, N. Liu, J. Xu, Y. Wang, X. Zhang, Stable black phosphorus encapsulation in porous mesh-like UiO-66 promoted charge transfer for photocatalytic oxidation of toluene and o-dichlorobenzene: performance, degradation pathway, and mechanism, ACS Catal. (2022) 8069–8081.

[5] Y. Wang, L. Ding, Q. Shi, S. Liu, L. Qian, Z. Yu, H. Wang, J. Lei, Z. Gao, H. Long, C. C. Xu, Volatile organic compounds (VOC) emissions control in iron ore sintering process: recent progress and future development, Chem. Eng. J. 448 (2022).

[6] X. Zhang, X. Miao, W. Xiang, J. Zhang, C. Cao, H. Wang, X. Hu, B. Gao, Ball milling biochar with ammonia hydroxide or hydrogen peroxide enhances its adsorption of phenyl volatile organic compounds (VOCs), J. Hazard. Mater. 403 (2021).

[7] J. Lee, J. Jang, J. Kim, S.-H. Lim, A recyclable indoor air filter system based on a photocatalytic metal-organic framework for the removal of harmful volatile organic compounds, Chem. Eng. J. 430 (2022).

[8] M. Kask, J. Bolobajev, M. Krichevskaya, Gas-phase photocatalytic degradation of acetone and toluene, and their mixture in the presence of ozone in continuous multi-section reactor as possible air post-treatment for exhaust from pulsed corona discharge, Chem. Eng. J. 399 (2020).

[9] O. Debono, V. Hequet, L. Le Coq, N. Locoge, F. Thevenet, VOC ternary mixture effect on ppb level photocatalytic oxidation: Removal kinetic, reaction intermediates and mineralization, Appl. Catal. B-Environ. 218 (2017) 359–369.

[10] C.-C. Wang, J.-R. Li, X.-L. Lv, Y.-Q. Zhang, G. Guo, Photocatalytic organic pollutants degradation in metal-organic frameworks, Energ. Environ. Sci. 7 (9) (2014) 2831–2867.

[11] C. Zhang, C. Xie, Y. Gao, X. Tao, C. Ding, F. Fan, H.-L. Jiang, Charge Separation by Creating Band Bending in Metal-Organic Frameworks for Improved Photocatalytic Hydrogen Evolution, Angew. Chem.-Int. Ed. (2022).

[12] X.-Y. Xu, C. Chu, H. Fu, X.-D. Du, P. Wang, W. Zheng, C.-C. Wang, Light-responsive UiO-66-$NH_2$/$Ag_3PO_4$ MOF-nanoparticle composites for the capture and release of sulfamethoxazole, Chem. Eng. J. 350 (2018) 436–444.

[13] K. Joyaramulu, F. Geyer, A. Schneemann, S. Kment, M. Otyepka, R. Zboril, D. Vollmer, R.A. Fischer, Hydrophobic metal-organic frameworks, Adv. Mater. 31 (32) (2019).

[14] W. Zhai, J. Wang, M. Wang, X. Du, S. Wei, Adsorption and separation of $CO_2$/$N_2$ in metal organic frameworks: a theoretical investigation, J. Inorg. Mater. 35 (6) (2020) 697–702.

[15] X. Zhang, G. Li, D. Wu, X. Li, N. Hu, J. Chen, G. Chen, Y. Wu, Recent progress in the design fabrication of metal-organic frameworks-based nanozymes and their applications to sensing and cancer therapy, Biosens. Bioelectron. 137 (2019) 178–198.

[16] H. Wang, W.P. Lustig, J. Li, Sensing and capture of toxic and hazardous gases and vapors by metal-organic frameworks, Chem. Soc. Rev. 47 (13) (2018) 4729–4756.

[17] J.-D. Xiao, L. Han, J. Luo, S.-H. Yu, H.-L. Jiang, Integration of plasmonic effects and schottky junctions into metal-organic framework composites: steering charge flow for enhanced visible-light photocatalysis, Angew. Chem.-Int. Ed. 57 (4) (2018) 1103–1107.

[18] X. Ma, H. Liu, W. Yang, G. Mao, L. Zheng, H.-L. Jiang, Modulating coordination environment of single-atom catalysts and their proximity to photosensitive units for boosting MOF photocatalysis, J. Am. Chem. Soc. 143 (31) (2021) 12220–12229.

[19] M. Jia, Q. Liu, W. Xiong, Z. Yang, C. Zhang, D. Wang, Y. Xiang, H. Peng, J. Tong, J. Cao, H. Xu, $Ti^{3+}$ self-doped $TiO_2$ nanotubes photoelectrode decorated with Ar-$Fe_2O_3$ derived from MIL-100(Fe): enhanced photo-electrocatalytic performance for antibiotic degradation, Appl. Catal. B-Environ. 310 (2022).

[20] C. Guo, M. Cheng, G. Zhang, W. Xiong, C. Zhou, B. Song, L. Du, L. Li, C. Tang, G. Wang, H. Liu, Degradation of organic contaminants by peroxymonosulfate activated with zeolitic imidazolate framework-based catalysts: performances, mechanisms and stability, Environ. Sci.-Nano 10 (6) (2023) 1528–1552.

[21] W. Xiao, M. Cheng, Y. Liu, J. Wang, G. Zhang, Z. Wei, L. Li, L. Du, G. Wang, H. Liu, Functional metal/carbon composites derived from metal-organic frameworks: insight into structures, properties, performances, and mechanisms, ACS Catal. (2023) 1759–1790.

[22] J.H. Cavka, S. Jakobsen, U. Olsbye, N. Guillou, C. Lamberti, S. Bordiga, K. P. Lillerud, A new zirconium inorganic building brick forming metal organic frameworks with exceptional stability, J. Am. Chem. Soc. 130 (42) (2008) 13850–13851.

[23] Z. Jiang, X. Xu, Y. Ma, H.S. Cho, D. Ding, C. Wang, J. Wu, P. Oleynikov, M. Jia, J. Cheng, Y. Zhou, O. Terasaki, T. Peng, L. Zan, H. Deng, Filling metal-organic framework mesopores with $TiO_2$ for $CO_2$ photoreduction, Nature 586 (7830) (2020) 549-+.

[24] M. Xu, D. Li, K. Sun, L. Jiao, C. Xie, C. Ding, H.-L. Jiang, Interfacial microenvironment modulation boosting electron transfer between metal nanoparticles and MOFs for enhanced photocatalysis, Angew. Chem.-Int. Ed. 60 (30) (2021) 16372–16376.

[25] H.-L. Zheng, S.-L. Huang, M.-B. Luo, Q. Wei, E.-X. Chen, L. He, Q. Lin, Photochemical in situ exfoliation of metal-organic frameworks for enhanced visible-light-driven $CO_2$ reduction, Angew. Chem.-Int. Ed. 59 (52) (2020) 23588–23592.

[26] K. Vellingiri, P. Kumar, A. Deep, K.-H. Kim, Metal-organic frameworks for the adsorption of gaseous toluene under ambient temperature and pressure, Chem. Eng. J. 307 (2017) 1116–1126.

[27] X. Zhang, Y. Yang, X. Lv, Y. Wang, N. Liu, D. Chen, L. Cui, Adsorption/desorption kinetics and breakthrough of gaseous toluene for modified microporous-mesoporous UiO-66 metal organic framework, J. Hazard. Mater. 366 (2019) 140–150.

[28] X. Qiu, Y. Zhang, Y. Zhu, C. Long, L. Su, S. Liu, Z. Tang, Applications of nanomaterials in asymmetric photocatalysis: recent progress, challenges, and opportunities, Adv. Mater. 33 (6) (2021).

[29] H. Furukawa, F. Gandara, Y.-B. Zhang, J. Jiang, W.L. Queen, M.R. Hudson, O. M. Yaghi, Water adsorption in porous metal-organic frameworks and related materials, J. Am. Chem. Soc. 136 (11) (2014) 4369–4381.

[30] S. Wang, M. Wahiduzzaman, L. Davis, A. Tissot, W. Shepard, J. Marrot, C. Martineau-Corcos, D. Hamdane, G. Maurin, S. Devautour-Vinot, C. Serre, A robust zirconium amino acid metal-organic framework for proton conduction, Nat. Commun. 9 (2018).

[31] F. Vermoortele, M. Maes, P.Z. Moghadam, M.J. Lennox, F. Ragon, M. Boulhout, S. Biswas, K.G.M. Laurier, I. Beurroies, R. Denoyel, M. Roeffaers, N. Stock, T. Dueren, C. Serre, D.E. De Vos, p-Xylene-selective metal-organic frameworks: a case of topology-directed selectivity, J. Am. Chem. Soc. 133 (46) (2011) 18526–18529.

[32] J. Yu, X. Wang, L. Chen, G. Lu, G. Shi, X. Xie, Y. Wang, J. Sun, Enhanced adsorption and visible-light photocatalytic degradation of toluene by CQDs/UiO-66 MOG with hierarchical pores, Chem. Eng. J. 435 (2022).

[33] G. Kresse, D. Joubert, From ultrasoft pseudopotentials to the projector augmented-wave method, Phys. Rev. B 59 (3) (1999) 1758–1775.

[34] J.P. Perdew, K. Burke, M. Ernzerhof, Generalized gradient approximation made simple, Phys. Rev. Lett. 77 (18) (1996) 3865–3868.

[35] P.E. Blochl, Projector augmented-wave method, Phys. Rev. B 50 (24) (1994) 17953–17979.

[36] K. Momma, F. Izumi, VESTA: a three-dimensional visualization system for electronic and structural analysis, J. Appl. Cryst. 41 (2008) 653–658.

[37] M.D. de Mello, G. Kumar, T. Tabassum, S.K. Jain, T.-H. Chen, S. Caratzoulas, X. Li, D.G. Vlachos, S.-I. Han, S.L. Scott, P. Dauenhauer, M. Tsapatsis, Phosphonate-modified UiO-66 bronsted acid catalyst and its use in dehydra-decyclization of 2-methyltetrahydrofuran to pentadienes, Angew. Chem.-Int. Ed. 59 (32) (2020) 13260–13266.

[38] J. Du, L. Chen, X. Zeng, S. Yu, W. Zhou, L. Tan, L. Dong, C. Zhou, J. Cheng, Hard-and-soft integration strategy for preparation of exceptionally stable Zr(Hf)-UiO-66 via thiol-ene click chemistry, ACS Appl. Mater. Interfaces 12 (25) (2020) 28576–28585.

[39] X. Zhang, Y. Yang, L. Song, J. Chen, Y. Yang, Y. Wang, Enhanced adsorption performance of gaseous toluene on defective UiO-66 metal organic framework: equilibrium and kinetic studies, J. Hazard. Mater. 365 (2019) 597–605.

[40] H. Wu, Y.S. Chua, V. Krungleviciute, M. Tyagi, P. Chen, T. Yildirim, W. Zhou, Unusual and highly tunable missing-linker defects in zirconium metal-organic framework UiO-66 and their important effects on gas adsorption, J. Am. Chem. Soc. 135 (28) (2013) 10525–10532.

[41] C. Xu, Y. Pan, G. Wan, H. Liu, L. Wang, H. Zhou, S.H. Yu, H.L. Jiang, Turning on visible-light photocatalytic C-H oxidation over metal-organic frameworks by introducing metal-to-cluster charge transfer, J. Am. Chem. Soc. 141 (48) (2019) 19110–19117.

[42] L. Xiao, Q. Zhang, P. Chen, L. Chen, F. Ding, J. Tang, Y.-J. Li, C.-T. Au, S.-F. Yin, Copper-mediated metal-organic framework as efficient photocatalyst for the partial oxidation of aromatic alcohols under visible-light irradiation: synergism of plasmonic effect and schottky junction, Appl. Catal. B-Environ. 248 (2019) 380–387.

[43] X.-H. Yi, S.-Q. Ma, X.-D. Du, C. Zhao, H. Fu, P. Wang, C.-C. Wang, The facile fabrication of 2D/3D Z-scheme g-$C_3N_4$/UiO-66 heterojunction with enhanced photocatalytic Cr(VI) reduction performance under white light, Chem. Eng. J. 375 (2019).

[44] W. Dong, D. Wang, H. Wang, M. Li, F. Chen, F. Jia, Q. Yang, X. Li, X. Yuan, J. Gong, H. Li, J. Ye, Facile synthesis of $In_2S_3$/UiO-66 composite with enhanced adsorption performance and photocatalytic activity for the removal of tetracycline under visible light irradiation, J. Colloid Interface Sci. 535 (2019) 444–457.

[45] J. Li, X.A. Dong, G. Zhang, W. Cui, W. Cen, Z. Wu, S.C. Lee, F. Dong, Probing ring-opening pathways for efficient photocatalytic toluene decomposition, J. Mater. Chem. A 7 (7) (2019) 3366–3374.

[46] H. Niu, K. Li, B. Chu, W. Su, J. Li, Heterogeneous reactions between toluene and $NO_2$ on mineral particles under simulated atmospheric conditions, Environ. Sci. Technol. 51 (17) (2017) 9596–9604.

[47] M.D. Hernandez-Alonso, I. Tejedor-Tejedor, J.M. Coronado, M.A. Anderson, Operando FTIR study of the photocatalytic oxidation of methylcyclohexane and toluene in air over $TiO_2$-$ZrO_2$ thin films: influence of the aromaticity of the target molecule on deactivation, Appl. Catal. B-Environ. 101 (3–4) (2011) 283–293.

[48] M. Jang, S.R. McDow, Products of benz a anthracene photodegradation in the presence of known organic constituents of atmospheric aerosols, Environ. Sci. Technol. 31 (4) (1997) 1046–1053.

[49] Y. Chen, S. Tong, J. Wang, C. Peng, M. Ge, X. Xie, J. Sun, Effect of titanium dioxide on secondary organic aerosol formation, Environ. Sci. Technol. 52 (20) (2018) 11612–11620.

[50] L. Chen, X. Wang, Z. Rao, Z. Tang, G. Shi, Y. Wang, G. Lu, X. Xie, D. Chen, J. Sun, One-pot synthesis of the MIL-100 (Fe) MOF/MOX homojunctions with tunable hierarchical pores for the photocatalytic removal of BTXS, Appl. Catal. B-Environ. 303 (2022).

[51] V.R. Bakuru, S.R. Churipard, S.P. Maradur, S.B. Kalidindi, Exploring the Bronsted acidity of UiO-66 (Zr, Ce, Hf) metal-organic frameworks for efficient solketal synthesis from glycerol acetalization, Dalton Trans. 48 (3) (2019) 843–847.

[52] P. Hu, X.P. Liang, M. Yaseen, X.D. Sun, Z.F. Tong, Z.X. Zhao, Preparation of highly-hydrophobic novel N-coordinated UiO-66(Zr) with dopamine via fast mechano-chemical method for (CHO-/Cl-)-VOCs competitive adsorption in humid environment, Chem. Eng. J. 332 (2018) 608–618.

[53] W. Zhang, W. Huang, J. Jin, Y. Gan, S. Zhang, Oxygen-vacancy-mediated energy transfer for singlet oxygen generation by diketone-anchored MIL-125, Appl. Catal. B-Environ. 292 (2021).

[54] Z. Rao, G. Lu, L. Chen, A. Mahmood, G. Shi, Z. Tang, X. Xie, J. Sun, Photocatalytic oxidation mechanism of gas-phase VOCs: unveiling the role of holes, ·OH and $\cdot O_2$-, Chem. Eng. J. 430 (2022).

[55] Y. Nosaka, A.Y. Nosaka, Generation and detection of reactive oxygen species in photocatalysis, Chem. Rev. 117 (17) (2017) 11302–11336.